Feasibility of Inferring Spatial Transcriptomics from Single-Cell Histological Patterns for Studying Colon Cancer Tumor Heterogeneity

Michael Y. Fatemi[1], Yunrui Lu[2], Zarif L. Azher[11,13*], Cyril Sharma[3], Eric Feng[4], Alos B. Diallo[2,5,6], Gokul Srinivasan[2], Grace M. Rosner[7,8], Kelli B. Pointer[7,8], Brock C. Christensen[5], Lucas A. Salas[5], Gregory J. Tsongalis[2], Scott M. Palisoul[2], Laurent Perreard[9], Fred W. Kolling IV[9], Louis J. Vaickus[2] and Joshua J. Levy[2,6,10,11,12]

[1]*University of Virginia, Charlottesville, Virginia, U.S.A.*
[2]*Emerging Diagnostic and Investigative Technologies, Department of Pathology and Laboratory Medicine, Dartmouth Health, Lebanon, NH, U.S.A.*
[3]*Department of Computer Science, Purdue University, West Lafayette, IN, U.S.A.*
[4]*Thomas Jefferson High School for Science and Technology, Alexandria, VA, U.S.A.*
[5]*Department of Epidemiology, Dartmouth College Geisel School of Medicine, Hanover, NH, U.S.A.*
[6]*Program in Quantitative Biomedical Sciences, Dartmouth College Geisel School of Medicine, Hanover, NH, U.S.A.*
[7]*Department of Medicine, Section of Radiology Oncology, Dartmouth Health, Lebanon, NH, U.S.A.*
[8]*Department of Molecular and Cell Biology, Dartmouth College Geisel School of Medicine, Hanover, NH, U.S.A.*
[9]*Genomics Shared Resource, Dartmouth Cancer Center, Lebanon, NH, U.S.A.*
[10]*Department of Dermatology, Dartmouth Health, Lebanon, NH, U.S.A.*
[11]*Department of Pathology and Laboratory Medicine, Cedars Sinai Medical Center, Los Angeles, CA, U.S.A.*
[12]*Department of Computational Biomedicine, Cedars Sinai Medical Center, Los Angeles, CA, U.S.A.*
[13]*Division of Biology and Biological Engineering, California Institute of Technology, Pasadena, CA, U.S.A.*

Keywords: Pathology, Cancer, Deep Learning, Spatial Transcriptomics, Histopathology.

Abstract: Spatial transcriptomics (ST) enables studying spatial organization of gene expression within tissues, offering insights into the molecular diversity of tumors. Recent methods have demonstrated the capability to disaggregate this information at subspot resolution by leveraging both expression and histological patterns. Elucidating such information from histology alone presents a significant challenge, but if solved can enable spatial molecular analysis at cellular resolution even where ST data is not available, reducing study costs. This study explores integrating single-cell histological and transcriptomic data to infer spatial mRNA expression patterns in colorectal cancer whole slide images. A cell-graph neural network algorithm was developed to align histological information extracted from detected cells with single cell RNA, facilitating the analysis of cellular groupings and gene relationships. We demonstrate that single-cell transcriptional heterogeneity within a spot could be predicted from histological markers extracted from cells detected within it. Our model exhibited proficiency in delineating overarching gene expression patterns across whole-slide images. This approach compared favorably to traditional computer vision methods which did not incorporate single cell expression during the model training. This innovative approach augments the resolution of spatial molecular assays utilizing histology as sole input through co-mapping of histological and transcriptomic datasets at the single-cell level.

1 INTRODUCTION

Cancer poses tremendous global burden on healthcare and quality of life. By the end of 2023, nearly 2 million new cancer cases and more than 600,000 cancer deaths will occur in the United States (Siegel et al., 2020, 2023). Colorectal cancer (CRC) is a particularly formidable solid tumor, with an annual incidence of approximately 150,000 new cases in the United States and a 63% 5-year survival rate (Siegel

[*] Denotes equal first authorship.

Fatemi, M. Y., Lu, Y., Azher, Z. L., Sharma, C., Feng, E., Diallo, A. B., Srinivasan, G., Rosner, G. M., Pointer, K. B., Christensen, B. C., Salas, L. A., Tsongalis, G. J., Palisoul, S. M., Perreard, L., Kolling IV, F. W., Vaickus, L. J. and Levy, J. J.
Feasibility of Inferring Spatial Transcriptomics from Single-Cell Histological Patterns for Studying Colon Cancer Tumor Heterogeneity.
DOI: 10.5220/0013157300003911

In *Proceedings of the 18th International Joint Conference on Biomedical Engineering Systems and Technologies (BIOSTEC 2025) - Volume 1*, pages 444-458
ISBN: 978-989-758-731-3; ISSN: 2184-4305

et al., 2020, 2023). With the shift in CRC to younger demographics and tumor metastasis being responsible for most cancer deaths, there is a pressing need for high-fidelity screening and prognostication (Cheng et al., 2022). The treasure trove of imaging and genomics information provided by nascent molecular assays and informatics techniques has the potential to inform more effective, targeted treatment options by revealing novel prognostic biomarkers.

Tumor Infiltrating Lymphocytes (TIL) are critical in modulating the Tumor Microenvironment (TME) and Tumor Immune Microenvironment (TIME) (de Visser & Joyce, 2023). The TME consists of malignant and benign cells, blood vessels, and extracellular matrix, interconnected through complex communication via cytokine recruitment factors (de Visser & Joyce, 2023). Recent studies highlight the importance of immune infiltrates, such as T cells, B cells, NK cells, and monocyte/lymphocyte cells, and their distribution, density, and relationships in mounting an effective anti-tumor response. For example, high levels of cytotoxic T cells within the tumor may indicate immune exhaustion (Collier et al., 2021). Understanding molecular changes and spatial arrangements associated with colon cancer metastasis is still incomplete, though several digital pathology assays have incorporated existing findings to serve as independent risk factors for recurrence. These assays include: 1) Immunoscore, which measures the density of cytotoxic T-cells at the tumor's invasive margin and inside the tumor (Galon et al., 2014), 2) CDX2, an epithelial marker of pluripotency indicating the tumor's ability to bypass immune response and growth inhibition checkpoints (Dalerba et al., 2016; Saad et al., 2011; Tarazona et al., 2020), and 3) circulating tumor DNA, such as mutations in the Vascular Endothelial Growth Factor (VEGF) pathway (G. Chen et al., 2021; H. Li et al., 2019). While these assays are predictive of recurrence risk, they provide only a limited perspective on tumor metastasis phenomenology.

Spatial omics technologies, like 10x Genomics Visium Spatial Transcriptomics (ST) or GeoMX Digital Spatial Profiling (DSP), have facilitated the simultaneous analysis of multiple biomarkers, including the whole transcriptome, with remarkable spatial resolution (K. H. Chen et al., 2015; Hu et al., 2021; Lewis et al., 2021; Moses & Pachter, 2022). These technologies have been applied to further characterize TIL subpopulations in TME. However, their clinical utility is limited due to high costs, low throughput, and limited reproducibility. In previous work, we demonstrated the feasibility of utilizing machine learning algorithms to extract TIL and spatial biology information from Hematoxylin and Eosin (H&E) stains. This can be a cost-effective and high-throughput digital biomarker that could be employed prospectively as an adjunct test similar to Immunoscore for recurrence risk assessment (Monjo et al., 2022; Zeng et al., 2022). We found that careful selection of algorithms is crucial to capture molecular alterations and pathways reflective of histomorphological changes or large-scale tissue architecture changes (Fatemi et al., 2023; Srinivasan et al., 2023).

Nevertheless, the resolution of these findings is currently restricted to the available resolution of Visium spots, typically around 50 microns, which aggregates expression data across a small number of cells (1-10 cells). Incorporating single-cell information, captured through the new Chromium Flex technology can improve characterization of spatial cellular heterogeneity to enhance the resolution of the Visium data. Recent advancements in profiling technologies, including 10x Flex and CytAssist assays, enable the profiling of single-cell transcriptomics (scRNASeq) on serial sections of formalin-fixed paraffin-embedded (FFPE) tissue. This has the potential to enhance the capacity to perform spatial assessments at single-cell resolution on diverse cohorts.

Existing technologies to increase the resolution of Visium data require both ST and histological information and do not operate on tissue images alone. Previous studies have made attempts to infer single-cell RNA sequencing (scRNA-seq) data from breast cancer tissue slide sections, improving the resolution of the data and enabling the identification of different cell types within the tissue (Choi & Kim, 2019). Others have made attempts to infer Visium ST expression patterns aggregated across several cells per spot using image classification techniques with some domain-specific adaptations. For example, recent studies have trained DenseNet-121 and InceptionV3 models to predict gene expression (B. He et al., 2020; Levy-Jurgenson et al., 2020), and another work used a custom convolutional layer along with a graph attention network and transformer model to share information between Visium spots (Zeng et al., 2022). While the Visium platform primarily provides low-resolution, aggregated expression measurements across cells contained within a 50-micron spot (Duan et al., 2022; J. Liu et al., 2022), single-cell analyses offer a more comprehensive view of cellular heterogeneity.

The primary goal of this study is to enhance the predictive capability of algorithms that infer ST data solely from histology images, capturing single-cell heterogeneity within a spot and their aggregate spot-level expression. To achieve this, we combine the precise locations of individual cells, as identified in whole cell images, with the granular data from single-cell RNA sequencing (scRNA-seq). This approach integrates histological details from localized nuclei within and around Visium spots with corresponding scRNA-seq profiles mapped to the same spots. By seamlessly merging these datasets, our framework stands extracts richer molecular insights from cells, facilitating a more accurate prediction of both Visium ST and individual cell information.

We develop attribution methods to examine the structural organizations of cells that are most correlated with the expression of specific genes. This can contribute to a better understanding tumor-immune microenvironment dynamics and potentially aid in developing prognostic tools for colorectal tumors. In this paper, we compare the accuracy of methods that use cells as features with conventional computer vision methods featured in our previous work. Importantly, this study does not claim to infer scRNASeq data at specific locations of individual cells. Rather, we demonstrate the ability to leverage single-cell information to enhance the expression prediction at Visium spots on held-out tissue slides. This research establishes a foundational workflow and conceptual framework for the future inference of such information.

2 RESULTS

2.1 Overview of Cells2RNA Framework: Bridging Histological Patterns with Single-Cell Expression

Cells2RNA was crafted to infer single-cell expression from discernible histological patterns in instances where spatial transcriptomics and single-cell data might be lacking (Figure 1). The challenge lies in deducing single-cell nuances solely from histological patterns surrounding pinpointed cells (Figure 2A). Prior research has been limited to interpreting aggregated spot-level data. Yet, when disaggregated to the individual cell level, a richer tapestry of heterogeneity emerges, which becomes our focal point for inference. The goal of this study is to derive molecular insights paralleling the depth of Visium-based investigations, but strictly from histological imaging.

Central to our approach is a co-mapping methodology where histological patterns detected at the cellular level are intricately aligned with single-cell expression data (Figure 1A). Spatial transcriptomics serves as an intermediary in this process: during training, single-cell RNASeq data is mapped to corresponding Visium spots (Figure 1B) where cells are located and acts as an inference target for the histological attributes derived from these located cells. Although this alignment might not be perfect, it closely mirrors genuine single-cell expression dynamics within each Visium spot.

Using Visium and paired 40X resolution whole slide imaging from a cohort of nine stage pT3 colorectal patients (see section “Data Collection and Preprocessing”), the co-mapping technique was benchmarked against patch-level models (Inceptionv3) and other CGNNs that utilize alternative information extraction methods. We assessed their performance on predicting spot-level expression, capturing cellular heterogeneity within spots (using Wasserstein distance), maintaining tissue architectural relationships, and pathway analysis.

2.2 Model Comparison

Overall, models have strong performance– selecting the top CGNN model per gene resulted in an AUROC of 0.8138 ± 0.0069 and Spearman's statistic of 0.5724 ± 0.0133 (Table 1). However, across all experiments, model performances did not appear significantly different from each other, though we noticed several important trends (Figure 3,4). CGNN models were on-par with the Inception model (AUC=0.8204 ± 0.0073). The most predictive cell-based model had an AUROC of 0.8093 ± 0.0083, similar to the InceptionV3 model's AUROC interval of 0.8204 ± 0.0073, which leveraged additional information beyond the cell's immediate neighborhood and may have also benefited from the built-in structural feature extraction of CNNs. There was high agreement in top-performing genes between CGNN methods using graph contrastive learning or single-cell penalization as compared to a CGNN with no penalization/pretraining (Appendix Figure 1, Appendix Table 1).

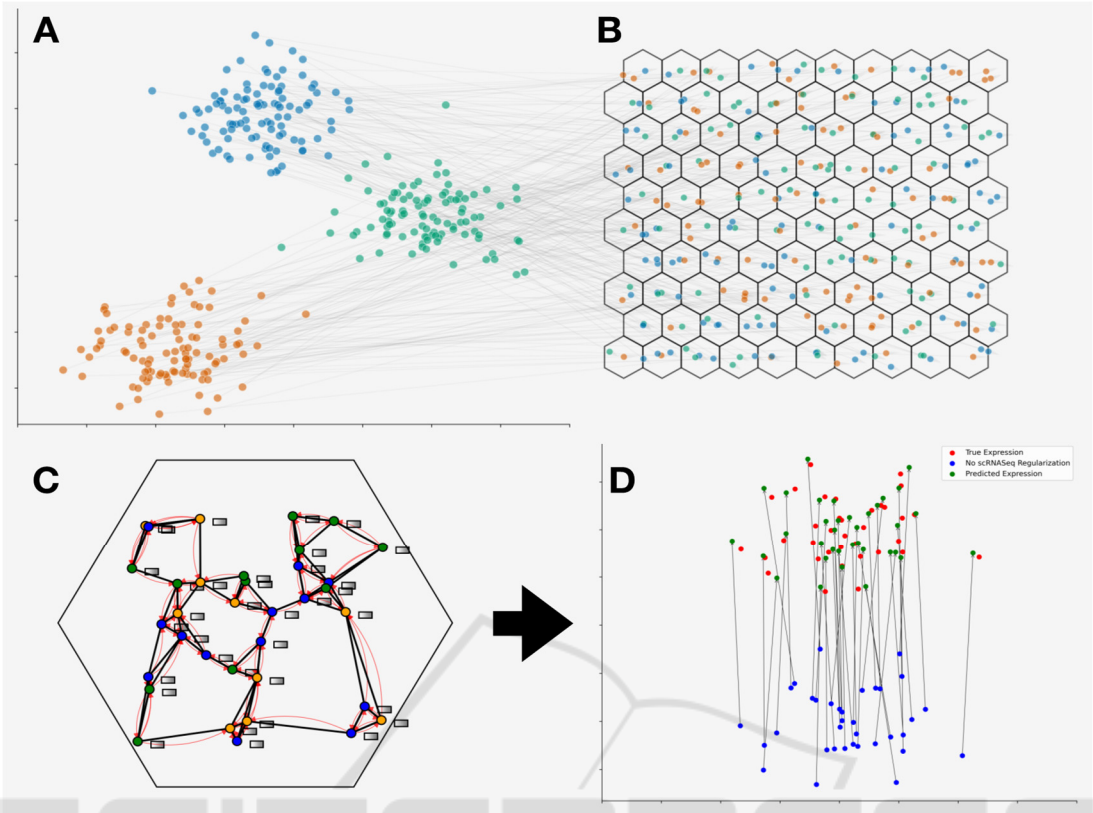

Figure 1: Overview of Cell2RNA's Co-Mapping Approach: (A) Low-dimensional visualization of single-cell RNA profiles, clusters indicating cell-type. (B) Spatial layout of identified cells across the tissue slide (assignment to spots represented by hexagons), color-coded by distinct gene expression patterns mapped from single cell profiles featured in (A). (C) In-depth view of cells located within a specific Visium spot, illustrating connectivity and cell relationships. Expression-related histological features, represented by grey rectangles, are shared among neighboring cells through red curves via a graph neural network. (D) A side-by-side low-dimensional comparison of scRNASeq profiles for a representative Visium spot: actual expression (red), model-predicted expression using the co-mapping training approach (green), and expression prediction without co-mapping training (blue).

Table 1: Comparison of model performance. Aggregate AUROC is calculated as the median AUROC across genes. Gene-level AUROC is calculated as the mean across cross-validation folds.

Modeling Approach	Spearman	AUROC	Optimal Transport (EMD)
Vanilla CGNN	0.5591 ± 0.0146	0.8093 ± 0.0083	0.2113 ± 0.0018
CGNN: Graph Contrastive Learning	0.5356 ± 0.0177	0.8049 ± 0.0083	0.1900 ± 0.0020
CGNN: Single-Cell Penalization	0.5381 ± 0.0158	0.8012 ± 0.0074	0.1473 ± 0.0018
CGNN: GCL and Single-cell penalization	0.5464 ± 0.0156	0.8084 ± 0.0093	0.1415 ± 0.0018
Top CGNN per Gene	0.5637 ± 0.0135	0.8138 ± 0.0069	N/A
Top Model per Gene	0.5766 ± 0.0122	0.8206 ± 0.0076	N/A
InceptionV3 (256x256)	0.5724 ± 0.0133	0.8204 ± 0.0073	N/A

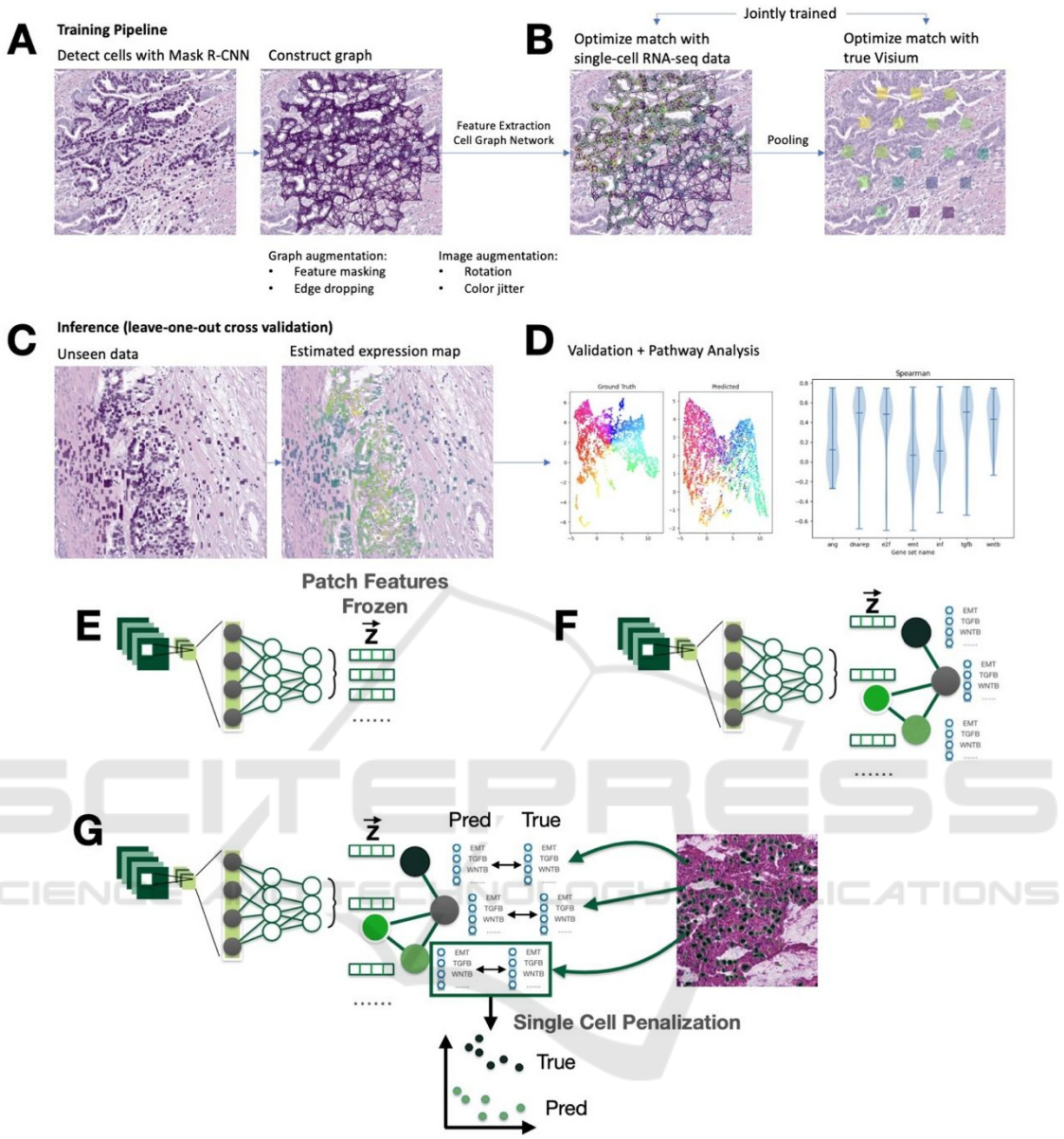

Figure 2: Schematic Representation of the Neural Network Workflow for Single-Cell Analysis. During the training phase, (A) a pre-trained Mask R-CNN model is applied to histology images to detect individual cells, after which a 6-nearest neighbors graph is constructed for the detected cells. (B) Features for each cell are extracted using a ResNet-50 neural network, and the aggregation of neighboring cell information is modeled using a Graph Attention Network (GAT). For each Visium spot, the node features are aggregated using sum pooling. (C) Pre-pooled node values are jointly optimized against single-cell RNA-sequencing (scRNA-seq) data, and (D) pooled Visium spot predictions are optimized against the corresponding ground truth data, using a mean-squared-error loss computed across log-transformed counts. (E)-(G) Visual description of neural network architectures and penalizations employed: (E) a two-stage neural network comprising a feature extraction stage and a prediction stage, this was not used in this work, (F) an end-to-end neural network encompassing the entire process from cell detection to feature extraction, graph convolutions and prediction, utilized in this study, and (G) the incorporation of single-cell-level penalties into the loss function to enforce consistent predictions with scRNA-seq data.

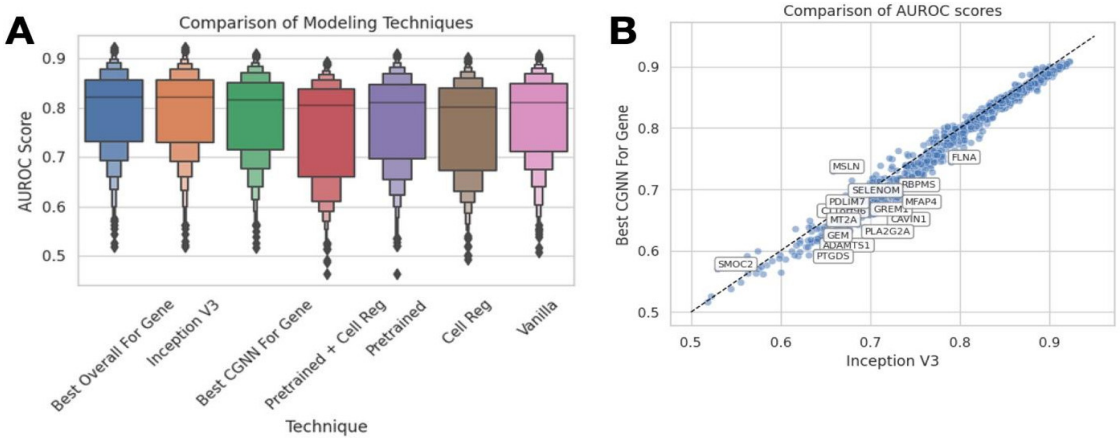

Figure 3: Performance comparison between methods. A) Boxplot of AUROC scores from each method; B) comparison of AUROC for best CGNN and CNN for each gene.

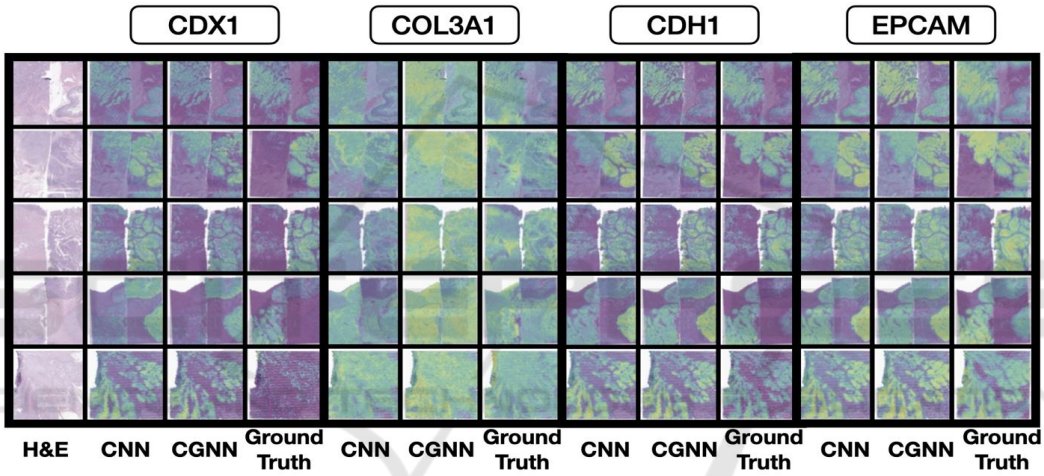

Figure 4: Predicted expression for various genes: CNN, CGNN, compared to ground truth for genes CDX1, COL3A1, CDH1 and EPCAM across sections from all nine patients.

2.3 Single-Cell Attribution Maps Point to Spatial Cellular Heterogeneity

Single-cell regularization significantly improved alignment of cellular information extracted from located cells, as measured by the Earth Mover's (Wasserstein) distance between cells assigned to spots using Tangram and their closest detected matches (EMD=0.1415 ± 0.0018 with penalization, 0.2113 ± 0.0018 without penalization). This improvement does not negatively impact AUROC. Cells were embedded using UMAP based on the ground truth and predicted expression, with and without penalization with scRNASeq. Visual inspection of these UMAP embeddings confirmed the quantitative results of differences in EMD (Appendix Figure 2), that single-cell penalization causes node-level predicted expression from cellular histomorphology for genes to more closely resemble the distribution of single-cell data assigned to the Visium spot.

Overall, more than 80% of the genes exhibited a positive correlation between ground truth and predicted single-cell expression when single-cell regularization was employed, compared to around 20-30% of the genes without such regularization was not used (Appendix Figure 3). As illustrated in Figure 5E-G, we juxtapose the predicted level of EPCAM expression for each cell against ground truth data from a Visium assay. Our model's predictions and the ground truth at cellular resolution are visually consistent (Figure 5A-D), corroborating the high accuracy reported in the previous section as well as the lower EMD reported through single-cell penalization.

2.4 Topological Consistency of Inferred Expression Patterns

Across all capture areas, predicted spot level expression clustered similarly to the true expression (Figure 6). However, overlaying the clusters assigned to ground truth embeddings over the predicted expression embeddings, we found that clusters were less separated and fuzzier than the ground truth. Nonetheless, overlaying cluster assignments across the whole slide image demonstrates the ability of these models to derive expression signatures that can delineate key histological architectures.

2.5 Pathway Analysis

To compare performance across prediction targets, we selected pathways from MSigDB's Hallmark Gene Sets (Liberzon et al., 2011; Subramanian et al., 2005) and reported average AUC for genes from these sets. Across modeling approaches, genes involved in DNA repair and E2F targets were predicted with higher performance as compared to other molecular pathways (Appendix Figure 4). Dysregulation of DNA repair can accelerate tumor progression (L. Li et al., 2021), and therefore accurately detecting the presence of relevant genes may be useful in prognostication. We did notice that for some pathways, e.g., Epithelial to Mesenchymal Transition, penalizing by single-cell expression led to some loss of performance in distinguishing these molecular signatures (Appendix Figure 4).

We performed a pathway analysis by subsetting the top 10% of genes per modeling approach for further analysis using the Enrichr software/database (E. Y. Chen et al., 2013; Xie et al., 2021). Notably, we found that the WNT in Epithelial to Mesenchymal Transition in Cancer pathway, a chief contributor to the migration and metastasis of cancer cells, and several pathways associated with desmosome assembly (which regulate intercellular adhesion between metastasizing cells) were among the top ten most statistically significant gene sets detected in all four techniques, and EPCAM in Cancer Cell Motility and Proliferation is a statistically significant gene set in all four techniques. The WNT in Epithelial to Mesenchymal Transition in Cancer pathway has an AUROC of 0.8686 ± 0.0273 for the Inception model and 0.8638 ± 0.0238 for the "vanilla" cell graph model.

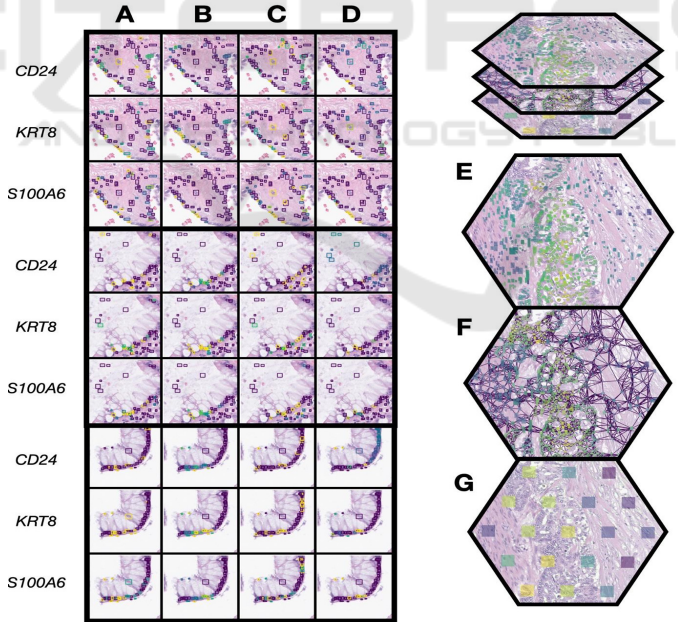

Figure 5: Alignment of True and Predicted Single-Cell and Visium-Spot Level Expression on a Histological Section. Illustration of the relationship between true and predicted single-cell expression on a histological section for genes CD24, KRT8, and S100A6. A) and C) display the ground truth of single-cell expression with and without single-cell regularization, respectively. B) and D) visualize the respective predicted single-cell expressions. Progressing from individual cellular predictions to a broader view, D)-G) detail the transition through EPCAM expression: from predicted cell-level expression in D) to an overarching cell graph across multiple Visium spots in E) and concluding with spot-level Visium expression in G).

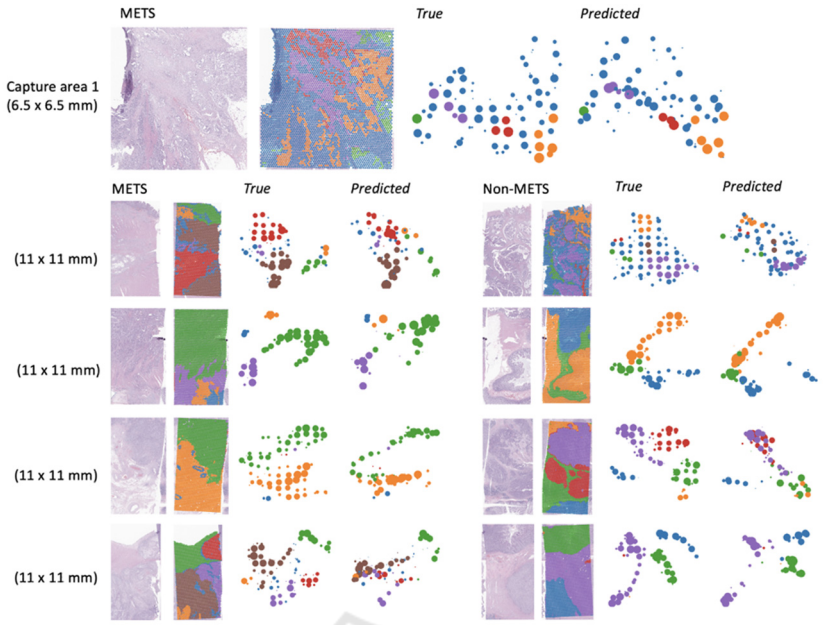

Figure 6: UMAP embeddings of tissue slides from selected capture areas, color-coded by HDBSCAN clusters. Comparisons include CGNN, CGNN with single-cell penalization, and patch-based methods against the ground truth. Clusters derived from the ground truth are overlaid on the slides for context. Patients with/without metastasis (METS) included.

3 DISCUSSION

Our primary objective was to draw inferences about spatial mRNA expression patterns from whole slide images (WSI), specifically by fusing single-cell histological and transcriptomic data. Instead of relying on expensive spatial molecular assays, our technique offers an economical avenue method which can subsequently aid in the risk evaluation of recurrence. Our results highlight the viability of utilizing spatial transcriptomics as a rich pretraining source, using scRNASeq to guide single-cell level interpretations that could benefit from graph-based representations.

Our study revealed that by considering cells' histomorphology and spatial relationships, we could effectively predict gene expression patterns across whole slide images. In some instances, these approaches outperformed traditional patch-based computer vision methods that analyze cropped images around each Visium spot. However, the predictive capacity of these approaches was found to be similar to patch-based methods, which is reasonable considering that the cells are contained within these patches and should present some loss of information. By explicitly incorporating cells as nested observations, attribution methods enabled the identification of structural cell organizations that exhibited the strongest correlation with the expression of specific genes.

3.1 Comparison of Cell-Level Approach to Patch-Based Methods

The performance of the CNN model does not surpass that of the cell-based approaches. Interestingly, our basic cell model demonstrates a bootstrapped AUROC confidence interval overlapping with that of the Inception model. This indicates that even when operating with potentially less diverse information like the extracellular matrix and connective tissue, the cell-based model remains competitive against its CNN counterpart. Although CNN may show a slight performance advantage, its insights are limited to single-pixel attributions, neglecting the broader scope of cell-cell interactions. Conversely, the GNN model offers superior explainability, permitting direct visualization of pivotal cell-cell interactions for particular genes and topological methods for deciphering important structural motifs.

3.2 Impact of Single-Cell Penalization

Single-cell penalization and contrastive pretraining showed minimal influence on the final outcome. This indicates that employing single-cell penalization can

shed light on the spatial nuances of cellular disparities without compromising performance. We believe this is due to the large dataset size (more than 60,000 Visium spots), which may mitigate the need or potential benefit of pretraining. Additionally, although we hoped that single-cell penalization would improve the model's robustness (by grounding predictions in real single-cell RNA quantification), the penalization provided modest performance gains over other methods. This suggests that models may produce the same optimum regardless of the intermediate feature values (i.e., cell-level predictions). Notably, single-cell data is not required during model inference as it is used solely for regularization during training

3.3 Revisiting Topological Consistency and Intermediate Histologically-Associated Molecular States

We discovered that although the predicted expression patterns mirrored the essential topological relationships tied to specific histological structures, they were more intertwined compared to the true expression, resulting in less pronounced clustering. Such mixed clustering might suggest that these clusters signify different degrees of cellular activity for various phenomena. It seems easier for machine learning models to distinguish between low and high activity levels, but interpolating intermediate levels of activity poses a challenge from a visual standpoint. Nevertheless, overall, the model's predictions are topologically in line with the ground truth. Areas of tissue with similar ground truth measurements also exhibit similar predicted expressions.

3.4 Reflections on Pathway Analysis and Immunological Considerations

The WNT in Epithelial to Mesenchymal Transition in Cancer and EPCAM in Cancer Cell Motility and Proliferation were notable pathways from the results section. Wnt/β-catenin signaling is implicated in cell differentiation and proliferation and has been implicated in increasing the number of "stem-like" cells in a tumor (Pai et al., 2017). EPCAM is responsible for modulating epithelial cell adhesion, and - while having conflicting trends in recent research - can result in adhesive and migratory cell activity, potentially impacting the potential for metastasis (Fagotto & Aslemarz, 2020).

Our approach to unveil single-cell heterogeneity from whole slide images through alignment with single-cell expression bears several important immunological implications. First, the spatial arrangement of immune cells not only influences processes governing the anti-tumoral response but may offer insights as to the efficacy of immunotherapies including checkpoint inhibitors which has been a timely subject of inquiry (Dermani et al., 2019, p. 1; X. Wang et al., 2022). Deciphering the spatial make-up may also further reveal how tumors can establish immunosuppressive environments or contribute to an immune exhaustion phenotype (Ando et al., 2020; Yang et al., 2019). These topics underscore work being done to study how tumors can alter their immunogenicity and immune evasion tactics, potentially informing CAR T-cell therapies or selection of specific antibodies which can be applied in a personalized manner (Z. Liu et al., 2022; Peng et al., 2022; F. Wang et al., 2023). Revealing additional heterogeneity may refine selection of adjuvant therapy choices outside of existing prognostic measures.

3.5 Limitations and Future Directions

Our study has several limitations that offer avenues for future research. First, while our cohort of nine samples is large for a Visium study, we plan to amass a larger, more diverse cohort to bolster the robustness of our findings by accounting for further tumor heterogeneity. As our cohort was restricted to pT3 patients, future work will examine the predictiveness of these algorithms at additional tumor sites and levels of TME invasiveness. Inaccurate mapping of single-cell profiles to Visium spots may have also impacted the validity of single-cell associations and could improve with the adoption of other spatial mapping methods. We will also investigate how performance of single cell disaggregation is different based on level of expression. Overall, our study signifies a crucial step towards improving cancer diagnostics and prognosis by incorporating spatial transcriptomics into histological images, and future efforts will focus on refining these techniques.

4 CONCLUSION

Our study revealed that by considering cell histomorphology and spatial relationships, we could effectively predict gene expression patterns across whole slide images and recover local patterns of cellular heterogeneity. Identifying structural cell organizations that exhibited the strongest correlation with the expression of specific genes has the potential

to drastically improve our understanding of the tumor-immune microenvironment and potentially guide personalized treatment. Future applications of this method could include predicting response to immunotherapy based on the spatial distribution and expression patterns of immune cells in the tumor microenvironment. Our work is a promising direction for enhancing not only the diagnosis and prognosis of cancer but also our broader understanding of the clinical and immunological intricacies of tumor microenvironments.

5 METHODS

5.1 Data Collection

The dataset used in this study comprised nine patients with pathologic T Stage-III (pT3) colorectal cancer. Following IRB approval, these patients were selected through a retrospective review of pathology reports from 2016 to 2019. Patients were matched based on various criteria such as age, sex, tumor grade, tissue size, mismatch repair/microsatellite instability (MMR/MSI/MSS) status, and tumor site, balanced representation across these factors. Specific regions of interest within these sections, including epithelium, tumor-invasive front, intratumoral areas, and lymphatics, were annotated by a board-certified GI pathologist. Following annotation, these regions were dissected from the tissue, and subjected to H&E staining, imaging, and Visium profiling at the Pathology Shared Resource at Dartmouth Cancer Center and Single Cell Genomics Core in the Center for Quantitative Biology.

To achieve uniform staining and enhance image quality, we incorporated the CytAssist workflow, which allows Visum profiling of tissues on standard histology slides, enabling the use of automated staining (Sakura Tissue-Tek Prisma Stainer– Sakura Finetek USA, Inc. 1750 West 214th Street, Torrance, CA 90501) and WSI at 40x resolution (0.25 micron per pixel) via Aperio GT450s to obtain high-quality images. Following the preparation of the tissue slides, we employed the Visium assay using the CytAssist technology according to the manufacturer's protocol (CG000495) (Rosasco et al., 2023). For data processing, we utilized Spaceranger V to align the CytAssist images with the corresponding 40X H&E stains, conduct quality control, and convert the Visium Spatial Transcriptomics (ST) data into genes expression matrices (Sun et al., 2020).

We utilized the Chromium Flex assay to acquire single-cell RNA-Seq data, specifically from serial sections of patients identified in Capture Areas 2 (left section) and 5 (right section), as detailed in Table 2. This method allows for single cell profiling of disaggregated FFPE tissue sections using the same transcriptomic probe set as the Visium assay, revealing the diverse cell types within the tissue. Data were processed using CellRanger v7.1.0 to generate quality control metrics and a cells by genes expression matrices for downstream processing. Notably, this single cell data was profiled from different serial sections than the Visium experiments.

5.2 Preprocessing and Augmentation

We curated a list of 1,000 target genes by initially filtering out those not appearing in at least 100 spots per patient. These genes were subsequently ranked based on the fraction of their spatial variance, as determined through SpatialDE analysis. To rectify aberrant gene expression levels, we applied a transformation to both prediction and target gene counts using the expression log(1 + counts).

Cell detection was performed using the Mask-RCNN framework, which was trained on both the Lizard dataset and our internal dataset (Graham et al., 2021; K. He et al., 2017; Vuola et al., 2019). The nuclei detection model, available through the public Detectron2 Model Zoo, served as our pre-trained base. This model was fineturned on our dataset for up to 5,000 epochs. After training, this cell detection model was systematically applied across each Whole Slide Image (WSI).

The associated image was normalized for each detected cell through standard scaling applied over the image channels. We implemented data augmentation techniques to enhance our dataset, including random rotations (up to 90º) and color jitter adjustments. These augmentations were specifically applied to the images and cell detections cropped around the Visium spots during the training phase.

5.3 Deep Learning to Integrate Information from Localized Cells to Predict Spatial Gene Expression

Cell graph neural networks (CGNN) facilitate the exchange of messages between adjacent cells, enabling the exchange/incorporation of contextual information (Jaume et al., 2021; Levy et al., 2021; M. M. Li et al., 2022; Reddy et al., 2022). This approach effectively captures the relationships between different cell populations within the tissue, including tumor cells and surrounding immune and other cell subpopulations. Leveraging these relationships can

enhance the predictive performance of our spatial RNA inference algorithms while providing additional information as to relevant cells for these predictions.

We implemented an end-to-end training strategy that integrates the simultaneous training of a Convolutional Neural Network (CNN) and a Graph Neural Network (GNN). The CNN is designed to extract cell-level features from histological images, while the GNN contextualizes these features by incorporating information from neighboring cells. Our end-to-end approach aims to harmonize the feature extraction and contextualization processes, enabling the CNN to learn cell-level features that are more effectively contextualized through iterative, integrated training with the GNN (Figure 1,2).

The backbone of the model is a four-layer graph attention network (GAT) (Raju et al., 2020; Veličković et al., 2018), which uses self-attention mechanisms to update the representation of each cell with the information of its neighbors. We extract nodal attributes from detected cells using a ResNet-50 model, which is trained jointly with the graph attention layers. The Euclidean distances between the spatial locations of detected cells are used to form k-nearest-neighbor cell graphs (k=6, determined through a sensitivity analysis). The model maps each cell to 512-dimensional vectors, and final node embeddings pass through a linear layer producing a vector representing each gene's relative pseudocount-transformed expression for each cell. Cells corresponding to the same Visium spot are aggregated through global sum pooling to predict expression for the spot. This is compared to the pseudocount-transformed ground-truth Visium data with mean squared error.

5.4 Comparison of Cell-Graph Neural Network Regularization Strategies

In addition to evaluating the congruence between ground truth and predicted expression at the spot level, we explored the following methodological variations:

1. Vanilla Supervised Learning Objective: This baseline approach focuses solely on the supervised learning objective, serving as a reference for evaluating the potential gains from additional regularization strategies.
2. Incorporating Graph Contrastive Learning: This approach introduces a self-supervised regularization term that encourages the model to learn embeddings through the comparison of augmented viewpoints of the same cell graph / Visium spot to different cell-graphs / Visium spot. This can enhance the model's sensitivity to spatial patterns in the data, potentially improving its predictive accuracy for spatial transcriptomics patterns.
3. Incorporating Single-Cell RNA-Seq Penalization through Optimal Transport: This strategy introduces a penalty term that encourages the model to align cell-level histological features more closely with corresponding single-cell RNA-Seq data. By leveraging optimal transport theory, this term effectively "guides" the model towards a solution where the spatial patterns inferred from histology are maximally consistent with independent single-cell RNA-Seq measurements, thereby enhancing the biological validity of the model's predictions.
4. Combining Graph Contrastive Learning and Single-Cell Penalization: This approach synergistically combines both the graph contrastive learning and the single-cell RNA-Seq penalization strategies, aiming to leverage the benefits of both spatial context awareness and alignment with single-cell RNA-Seq data. This dual-regularization strategy is designed to promote a model that is both sensitive to spatial patterns and tightly aligned with independent molecular measurements, potentially offering a balance between spatial sensitivity and biological validity.

5.5 Graph Contrastive Learning

Using the PyGCL package, graph contrastive learning was implemented through augmentations to random cell positions in the nearest neighbor graph construction, dropping edges with a probability of 0.1, and masking out features with a probability of 0.3. Graph contrastive learning is a form of self-supervised learning that can improve the generalizability and robustness of graphs (Qiu et al., 2020; Zhu et al., 2021). By intentionally adding noise to the training cell graphs and comparing these representations at different Visium spots, we aimed to improve the model's generalizability when tested on held-out data.

5.6 Incorporating Single Cell Expression

By encouraging the predictions derived from histological images of individual cells to align closely with the corresponding true single-cell expression profiles, we aim to enhance the interpretability of our models through more consistent and biologically meaningful cellular information, and increase the likelihood that our predictions accurately reflect the

true cellular composition at each spatial location. Single-cell profiles are only utilized during model training, and are not needed during ultimate inference.

We initiated our analysis by mapping scRNA profiles to Visium spots using Tangram (Biancalani et al., 2021), and we selected the top k most likely cells to be assigned to each spot, where k represents the number of detected cells in that spot. Tangram generates unique 1:1 mappings from single cell expression profiles to spatial transcriptomics spots based on transcriptomic similarity. We leveraged the Wasserstein loss – which measures the work required to transform one distribution into another (Flamary et al., 2021; Villani, 2009) – as an effective metric for aligning our predictive single-cell expression profiles with the true expression profiles derived from scRNA data.

5.7 Comparison to Convolutional Neural Network Approaches

The CGNN approaches were compared to patch-based convolutional neural network methodologies deemed highly predictive from previous works – namely the InceptionV3 neural network trained on images of tissue patches encompassing multiple cells inclusive of surrounding tissue architecture. We initialize the model with ImageNet weights (with the final layer truncated) and apply the same visual transformations as for the cell embeddings.

5.8 Training and Validation

CGNN models were implemented with the torch-geometric Python package (Fey & Lenssen, 2019). We use PyGCL (Zhu et al., 2021) to apply graph augmentations. CGNN were trained using the Adam optimizer (Kingma & Ba, 2017) with a learning rate of 0.0001 on one Nvidia V100, quickly converging after two epochs. Similarly, the CNN model was trained for around 100000 iterations on a Nvidia V100 GPU.

The final performances of these models were compared using leave-one-patient-out cross-validation. Statistics are reported with the Spearman correlation coefficients. We also sought to assess the performance of predicting binary gene expression (low/high), by dichotomizing expression according to (Levy-Jurgenson et al., 2020). We used this to calculate the area under the receiver operating characteristic curve (AUROC) as another performance measure. Performance statistics were generated for each cross-validation fold, including Spearman's correlation coefficients and area under the receiver operating characteristic curves (AUROCs) by gene. The results were then averaged across all folds to assess the best-performing model on a gene-specific basis. We calculated 95% confidence intervals for all performance statistics, reported using 1000 sample non-parametric bootstrapping.

5.9 Model Interpretation Through Gene Embedding and Pathway Analysis

We sought to understand how well each approach could recapitulate the relationships between the Visium spots. This was accomplished by applying Uniform Manifold Approximation and Projection (UMAP) to each predicted expression profile (McInnes et al., 2018). Each method's predicted and actual gene expressions were aligned and clustered using the AlignedUMAP method. Clusters determined by running HDBSCAN (McInnes et al., 2017) on the ground truth expression data were overlaid on top of the UMAP plots for the other methods. Then, we annotated each of our prediction points with the corresponding HDBSCAN cluster of the ground truth and performed an aligned UMAP, jointly minimizing the distance between similar expressions in the embedding space and between paired ground truth and true locations. In addition, we annotated our histology images with the HBDSCAN clusters to interpret the tissue type of origin for each point.

Pathway analyses were performed to assess the ability of the methods to capture broader biological phenomena. We used separate methods: 1) aggregating the Spearman correlation and AUROC statistics across genes associated with pathways identified from the MSigDB Hallmarks gene set, and 2) evaluating the enrichment of the highest genes as ranked using their performance statistics, utilizing enrichR, which employs a modified Fisher's exact test. By examining the average performance across pathway analysis and overlap tests for the top-performing genes, we can gain insights into which biological phenomena each method effectively represents.

DECLARATIONS

Ethics Approval, Funding, Acknowledgements

Ethics approval and consent to participate: Human Research Protection Program IRB of Dartmouth Health gave ethical approval for this work.

JL is supported by Department of Defense grant 545 PR220927, and NIH awards P20GM130454, 546 P20GM104416, R24GM141194, R01CA277810.

This study was carried out in the Genomics and Molecular Biology Shared Resource (GMBSR) at Dartmouth which is supported by NCI Cancer Center Support Grant 5P30CA023108 and NIH S10 (1S10OD030242) awards. Single cell studies were conducted through the Dartmouth Center for Quantitative Biology in collaboration with the GMBSR with support from NIGMS (P20GM130454) and NIH S10 (S10OD025235) awards.

REFERENCES

Ando, M., Ito, M., Srirat, T., Kondo, T., & Yoshimura, A. (2020). Memory T cell, exhaustion, and tumor immunity. Immunological Medicine, 43(1), 1–9. https://doi.org/10.1080/25785826.2019.1698261

Biancalani, T., Scalia, G., Buffoni, L., Avasthi, R., Lu, Z., Sanger, A., Tokcan, N., Vanderburg, C. R., Segerstolpe, Å., Zhang, M., Avraham-Davidi, I., Vickovic, S., Nitzan, M., Ma, S., Subramanian, A., Lipinski, M., Buenrostro, J., Brown, N. B., Fanelli, D., … Regev, A. (2021). Deep learning and alignment of spatially resolved single-cell transcriptomes with Tangram. Nature Methods, 18(11), Article 11. https://doi.org/10.1038/s41592-021-01264-7

Chen, E. Y., Tan, C. M., Kou, Y., Duan, Q., Wang, Z., Meirelles, G. V., Clark, N. R., & Ma'ayan, A. (2013). Enrichr: Interactive and collaborative HTML5 gene list enrichment analysis tool. BMC Bioinformatics, 14(1), 128. https://doi.org/10.1186/1471-2105-14-128

Chen, G., Peng, J., Xiao, Q., Wu, H.-X., Wu, X., Wang, F., Li, L., Ding, P., Zhao, Q., Li, Y., Wang, D., Shao, Y., Bao, H., Pan, Z., Ding, K.-F., Cai, S., Wang, F., & Xu, R.-H. (2021). Postoperative circulating tumor DNA as markers of recurrence risk in stages II to III colorectal cancer. Journal of Hematology & Oncology, 14(1), 80. https://doi.org/10.1186/s13045-021-01089-z

Chen, K. H., Boettiger, A. N., Moffitt, J. R., Wang, S., & Zhuang, X. (2015). Spatially resolved, highly multiplexed RNA profiling in single cells. Science, 348(6233). https://doi.org/10.1126/science.aaa6090

Cheng, E., Ou, F.-S., Ma, C., Spiegelman, D., Zhang, S., Zhou, X., Bainter, T. M., Saltz, L. B., Niedzwiecki, D., & Mayer, R. J. (2022). Diet-and Lifestyle-Based Prediction Models to Estimate Cancer Recurrence and Death in Patients With Stage III Colon Cancer (CALGB 89803/Alliance). Journal of Clinical Oncology, JCO-21.

Choi, Y. H., & Kim, J. K. (2019). Dissecting Cellular Heterogeneity Using Single-Cell RNA Sequencing. Molecules and Cells, 42(3), 189–199. https://doi.org/10.14348/molcells.2019.2446

Collier, J. L., Weiss, S. A., Pauken, K. E., Sen, D. R., & Sharpe, A. H. (2021). Not-so-opposite ends of the spectrum: CD8+ T cell dysfunction across chronic infection, cancer and autoimmunity. Nature Immunology, 22(7), Article 7. https://doi.org/10.1038/s41590-021-00949-7

Dalerba, P., Sahoo, D., Paik, S., Guo, X., Yothers, G., Song, N., Wilcox-Fogel, N., Forgó, E., Rajendran, P. S., Miranda, S. P., Hisamori, S., Hutchison, J., Kalisky, T., Qian, D., Wolmark, N., Fisher, G. A., van de Rijn, M., & Clarke, M. F. (2016). CDX2 as a Prognostic Biomarker in Stage II and Stage III Colon Cancer. The New England Journal of Medicine, 374(3), 211–222. https://doi.org/10.1056/NEJMoa1506597

de Visser, K. E., & Joyce, J. A. (2023). The evolving tumor microenvironment: From cancer initiation to metastatic outgrowth. Cancer Cell, 41(3), 374–403.

Dermani, F. K., Samadi, P., Rahmani, G., Kohlan, A. K., & Najafi, R. (2019). PD-1/PD-L1 immune checkpoint: Potential target for cancer therapy. Journal of Cellular Physiology, 234(2), 1313–1325. https://doi.org/10.1002/jcp.27172

Duan, H., Cheng, T., & Cheng, H. (2022). Spatially resolved transcriptomics: Advances and applications. Blood Science, 5(1), 1–14. https://doi.org/10.1097/BS9.0000000000000141

Fagotto, F., & Aslemarz, A. (2020). EpCAM cellular functions in adhesion and migration, and potential impact on invasion: A critical review. Biochimica et Biophysica Acta (BBA) - Reviews on Cancer, 1874(2), 188436. https://doi.org/10.1016/j.bbcan.2020.188436

Fatemi, M., Feng, E., Sharma, C., Azher, Z., Goel, T., Ramwala, O., Palisoul, S. M., Barney, R. E., Perreard, L., Kolling, F. W., Salas, L. A., Christensen, B. C., Tsongalis, G. J., Vaickus, L. J., & Levy, J. J. (2023). Inferring spatial transcriptomics markers from whole slide images to characterize metastasis-related spatial heterogeneity of colorectal tumors: A pilot study. Journal of Pathology Informatics, 14, 100308. https://doi.org/10.1016/j.jpi.2023.100308

Fey, M., & Lenssen, J. E. (2019). Fast Graph Representation Learning with PyTorch Geometric. arXiv:1903.02428 [Cs, Stat]. http://arxiv.org/abs/1903.02428

Flamary, R., Courty, N., Gramfort, A., Alaya, M. Z., Boisbunon, A., Chambon, S., Chapel, L., Corenflos, A., Fatras, K., & Fournier, N. (2021). Pot: Python optimal transport. Journal of Machine Learning Research, 22(78), 1–8.

Galon, J., Mlecnik, B., Bindea, G., Angell, H. K., Berger, A., Lagorce, C., Lugli, A., Zlobec, I., Hartmann, A., Bifulco, C., Nagtegaal, I. D., Palmqvist, R., Masucci, G. V., Botti, G., Tatangelo, F., Delrio, P., Maio, M., Laghi, L., Grizzi, F., … Pagès, F. (2014). Towards the introduction of the 'Immunoscore' in the classification of malignant tumours. The Journal of Pathology, 232(2), 199–209. https://doi.org/10.1002/path.4287

Graham, S., Jahanifar, M., Azam, A., Nimir, M., Tsang, Y.-W., Dodd, K., Hero, E., Sahota, H., Tank, A., & Benes, K. (2021). Lizard: A large-scale dataset for colonic nuclear instance segmentation and classification. Proceedings of the IEEE/CVF International Conference on Computer Vision, 684–693.

https://openaccess.thecvf.com/content/ICCV2021W/CDPath/html/Graham_Lizard_A_Large-Scale_Dataset_for_Colonic_Nuclear_Instance_Segmentation_and_ICCVW_2021_paper.html

He, B., Bergenstråhle, L., Stenbeck, L., Abid, A., Andersson, A., Borg, Å., Maaskola, J., Lundeberg, J., & Zou, J. (2020). Integrating spatial gene expression and breast tumour morphology via deep learning. Nature Biomedical Engineering, 4(8), 827–834. https://doi.org/10.1038/s41551-020-0578-x

He, K., Gkioxari, G., Dollár, P., & Girshick, R. (2017). Mask r-cnn. Proceedings of the IEEE International Conference on Computer Vision, 2961–2969. http://openaccess.thecvf.com/content_iccv_2017/html/He_Mask_R-CNN_ICCV_2017_paper.html

Hu, J., Schroeder, A., Coleman, K., Chen, C., Auerbach, B. J., & Li, M. (2021). Statistical and machine learning methods for spatially resolved transcriptomics with histology. Computational and Structural Biotechnology Journal, 19, 3829–3841. https://doi.org/10.1016/j.csbj.2021.06.052

Jaume, G., Pati, P., Anklin, V., Foncubierta, A., & Gabrani, M. (2021). Histocartography: A toolkit for graph analytics in digital pathology. MICCAI Workshop on Computational Pathology, 117–128.

Kingma, D. P., & Ba, J. (2017). Adam: A Method for Stochastic Optimization (arXiv:1412.6980). arXiv. https://doi.org/10.48550/arXiv.1412.6980

Levy, J., Haudenschild, C., Barwick, C., Christensen, B., & Vaickus, L. (2021). Topological Feature Extraction and Visualization of Whole Slide Images using Graph Neural Networks. Pacific Symposium on Biocomputing. Pacific Symposium on Biocomputing, 26, 285–296.

Levy-Jurgenson, A., Tekpli, X., Kristensen, V. N., & Yakhini, Z. (2020). Spatial transcriptomics inferred from pathology whole-slide images links tumor heterogeneity to survival in breast and lung cancer. Scientific Reports, 10(1), 18802. https://doi.org/10.1038/s41598-020-75708-z

Lewis, S. M., Asselin-Labat, M.-L., Nguyen, Q., Berthelet, J., Tan, X., Wimmer, V. C., Merino, D., Rogers, K. L., & Naik, S. H. (2021). Spatial omics and multiplexed imaging to explore cancer biology. Nature Methods, 18(9), 997–1012.

Li, H., Jing, C., Wu, J., Ni, J., Sha, H., Xu, X., Du, Y., Lou, R., Dong, S., & Feng, J. (2019). Circulating tumor DNA detection: A potential tool for colorectal cancer management (Review). Oncology Letters, 17(2), 1409–1416. https://doi.org/10.3892/ol.2018.9794

Li, L., Guan, Y., Chen, X., Yang, J., & Cheng, Y. (2021). DNA Repair Pathways in Cancer Therapy and Resistance. Frontiers in Pharmacology, 11. https://www.frontiersin.org/articles/10.3389/fphar.2020.629266

Li, M. M., Huang, K., & Zitnik, M. (2022). Graph representation learning in biomedicine and healthcare. Nature Biomedical Engineering, 1–17.

Liberzon, A., Subramanian, A., Pinchback, R., Thorvaldsdóttir, H., Tamayo, P., & Mesirov, J. P. (2011). Molecular signatures database (MSigDB) 3.0. Bioinformatics, 27(12), 1739–1740. https://doi.org/10.1093/bioinformatics/btr260

Liu, J., Tran, V., Vemuri, V. N. P., Byrne, A., Borja, M., Kim, Y. J., Agarwal, S., Wang, R., Awayan, K., Murti, A., Taychameekiatchai, A., Wang, B., Emanuel, G., He, J., Haliburton, J., Oliveira Pisco, A., & Neff, N. F. (2022). Concordance of MERFISH spatial transcriptomics with bulk and single-cell RNA sequencing. Life Science Alliance, 6(1), e202201701. https://doi.org/10.26508/lsa.202201701

Liu, Z., Zhou, Z., Dang, Q., Xu, H., Lv, J., Li, H., & Han, X. (2022). Immunosuppression in tumor immune microenvironment and its optimization from CAR-T cell therapy. Theranostics, 12(14), 6273.

McInnes, L., Healy, J., & Astels, S. (2017). hdbscan: Hierarchical density based clustering. Journal of Open Source Software, 2(11), 205. https://doi.org/10.21105/joss.00205

McInnes, L., Healy, J., Saul, N., & Großberger, L. (2018). UMAP: Uniform Manifold Approximation and Projection. Journal of Open Source Software, 3(29), 861. https://doi.org/10.21105/joss.00861

Monjo, T., Koido, M., Nagasawa, S., Suzuki, Y., & Kamatani, Y. (2022). Efficient prediction of a spatial transcriptomics profile better characterizes breast cancer tissue sections without costly experimentation. Scientific Reports, 12(1), 4133. https://doi.org/10.1038/s41598-022-07685-4

Moses, L., & Pachter, L. (2022). Museum of spatial transcriptomics. Nature Methods, 19(5), 534–546. https://doi.org/10.1038/s41592-022-01409-2

Pai, S. G., Carneiro, B. A., Mota, J. M., Costa, R., Leite, C. A., Barroso-Sousa, R., Kaplan, J. B., Chae, Y. K., & Giles, F. J. (2017). Wnt/beta-catenin pathway: Modulating anticancer immune response. Journal of Hematology & Oncology, 10(1), 101. https://doi.org/10.1186/s13045-017-0471-6

Peng, Z., Ye, M., Ding, H., Feng, Z., & Hu, K. (2022). Spatial transcriptomics atlas reveals the crosstalk between cancer-associated fibroblasts and tumor microenvironment components in colorectal cancer. Journal of Translational Medicine, 20(1), 302. https://doi.org/10.1186/s12967-022-03510-8

Qiu, J., Chen, Q., Dong, Y., Zhang, J., Yang, H., Ding, M., Wang, K., & Tang, J. (2020). Gcc: Graph contrastive coding for graph neural network pre-training. Proceedings of the 26th ACM SIGKDD International Conference on Knowledge Discovery & Data Mining, 1150–1160.

Raju, A., Yao, J., Haq, M. M., Jonnagaddala, J., & Huang, J. (2020). Graph Attention Multi-instance Learning for Accurate Colorectal Cancer Staging. Medical Image Computing and Computer Assisted Intervention – MICCAI 2020: 23rd International Conference, Lima, Peru, October 4–8, 2020, Proceedings, Part V, 529–539. https://doi.org/10.1007/978-3-030-59722-1_51

Reddy, R., Reddy, R., Sharma, C., Jackson, C., Palisoul, S., Barney, R., Kolling, F., Salas, L., Christensen, B., Brooks, G., Tsongalis, G., Vaickus, L., & Levy, J.

(2022). Graph Neural Networks Ameliorate Potential Impacts of Imprecise Large-Scale Autonomous Immunofluorescence Labeling of Immune Cells on Whole Slide Images. Proceedings of the First International Workshop on Geometric Deep Learning in Medical Image Analysis, 15–33. https://proceedings.mlr.press/v194/reddy22a.html

Rosasco, M. G., Ho, C.-S., Luo, T., Stein, M. M., Lonini, L., Stumpe, M. C., Venkataraman, J., Khare, S., & Salahudeen, A. A. (2023). Abstract 4692: Comparison of interassay similarity and cellular deconvolution in spatial transcriptomics data using Visum CytAssist. Cancer Research, 83(7_Supplement), 4692. https://doi.org/10.1158/1538-7445.AM2023-4692

Saad, R. S., Ghorab, Z., Khalifa, M. A., & Xu, M. (2011). CDX2 as a marker for intestinal differentiation: Its utility and limitations. World Journal of Gastrointestinal Surgery, 3(11), 159–166. https://doi.org/10.4240/wjgs.v3.i11.159

Siegel, R. L., Miller, K. D., Goding Sauer, A., Fedewa, S. A., Butterly, L. F., Anderson, J. C., Cercek, A., Smith, R. A., & Jemal, A. (2020). Colorectal cancer statistics, 2020. CA: A Cancer Journal for Clinicians, 70(3), 145–164.

Siegel, R. L., Miller, K. D., Wagle, N. S., & Jemal, A. (2023). Cancer statistics, 2023. CA: A Cancer Journal for Clinicians, 73(1), 17–48. https://doi.org/10.3322/caac.21763

Srinivasan, G., Davis, M., LeBoeuf, M., Fatemi, M., Azher, Z., Lu, Y., Diallo, A., Montivero, M. S., Kolling, F., Perrard, L., Salas, L., Christensen, B., Palisoul, S., Tsongalis, G., Vaickus, L., Preum, S., & Levy, J. (2023). Potential to Enhance Large Scale Molecular Assessments of Skin Photoaging through Virtual Inference of Spatial Transcriptomics from Routine Staining (p. 2023.07.30.551188). bioRxiv. https://doi.org/10.1101/2023.07.30.551188

Subramanian, A., Tamayo, P., Mootha, V. K., Mukherjee, S., Ebert, B. L., Gillette, M. A., Paulovich, A., Pomeroy, S. L., Golub, T. R., Lander, E. S., & Mesirov, J. P. (2005). Gene set enrichment analysis: A knowledge-based approach for interpreting genome-wide expression profiles. Proceedings of the National Academy of Sciences, 102(43), 15545–15550. https://doi.org/10.1073/pnas.0506580102

Sun, S., Zhu, J., & Zhou, X. (2020). Statistical analysis of spatial expression patterns for spatially resolved transcriptomic studies. Nature Methods, 17(2), Article 2. https://doi.org/10.1038/s41592-019-0701-7

Tarazona, N., Gimeno-Valiente, F., Gambardella, V., Huerta, M., Roselló, S., Zuniga, S., Calon, A., Carbonell-Asins, J. A., Fontana, E., Martinez-Ciarpaglini, C., Eason, K., Rentero-Garrido, P., Fleitas, T., Papaccio, F., Moro-Valdezate, D., Nyamundanda, G., Castillo, J., Espí, A., Sadanandam, A., … Cervantes, A. (2020). Detection of postoperative plasma circulating tumour DNA and lack of CDX2 expression as markers of recurrence in patients with localised colon cancer. ESMO Open, 5(5), e000847. https://doi.org/10.1136/esmoopen-2020-000847

Veličković, P., Cucurull, G., Casanova, A., Romero, A., Liò, P., & Bengio, Y. (2018). Graph Attention Networks. arXiv:1710.10903 [Cs, Stat]. http://arxiv.org/abs/1710.10903

Villani, C. (2009). Optimal Transport (Vol. 338). Springer Berlin Heidelberg. https://doi.org/10.1007/978-3-540-71050-9

Vuola, A. O., Akram, S. U., & Kannala, J. (2019). Mask-RCNN and U-Net Ensembled for Nuclei Segmentation. 2019 IEEE 16th International Symposium on Biomedical Imaging (ISBI 2019), 208–212. https://doi.org/10.1109/ISBI.2019.8759574

Wang, F., Long, J., Li, L., Wu, Z.-X., Da, T.-T., Wang, X.-Q., Huang, C., Jiang, Y.-H., Yao, X.-Q., Ma, H.-Q., Lian, Z.-X., Zhao, Z.-B., & Cao, J. (2023). Single-cell and spatial transcriptome analysis reveals the cellular heterogeneity of liver metastatic colorectal cancer. Science Advances, 9(24), eadf5464. https://doi.org/10.1126/sciadv.adf5464

Wang, X., Barrera, C., Bera, K., Viswanathan, V. S., Azarianpour-Esfahani, S., Koyuncu, C., Velu, P., Feldman, M. D., Yang, M., Fu, P., Schalper, K. A., Mahdi, H., Lu, C., Velcheti, V., & Madabhushi, A. (2022). Spatial interplay patterns of cancer nuclei and tumor-infiltrating lymphocytes (TILs) predict clinical benefit for immune checkpoint inhibitors. Science Advances, 8(22), eabn3966. https://doi.org/10.1126/sciadv.abn3966

Xie, Z., Bailey, A., Kuleshov, M. V., Clarke, D. J. B., Evangelista, J. E., Jenkins, S. L., Lachmann, A., Wojciechowicz, M. L., Kropiwnicki, E., Jagodnik, K. M., Jeon, M., & Ma'ayan, A. (2021). Gene Set Knowledge Discovery with Enrichr. Current Protocols, 1(3), e90. https://doi.org/10.1002/cpz1.90

Yang, L., Li, A., Lei, Q., & Zhang, Y. (2019). Tumor-intrinsic signaling pathways: Key roles in the regulation of the immunosuppressive tumor microenvironment. Journal of Hematology & Oncology, 12(1), 125. https://doi.org/10.1186/s13045-019-0804-8

Zeng, Y., Wei, Z., Yu, W., Yin, R., Yuan, Y., Li, B., Tang, Z., Lu, Y., & Yang, Y. (2022). Spatial transcriptomics prediction from histology jointly through Transformer and graph neural networks. Briefings in Bioinformatics, 23(5), bbac297. https://doi.org/10.1093/bib/bbac297

Zhu, Y., Xu, Y., Liu, Q., & Wu, S. (2021). An empirical study of graph contrastive learning. arXiv Preprint arXiv:2109.01116.

APPENDIX

Appendix materials can be found at: https://zenodo.org/records/14538826.